

Three Years of Atmospheric Characterization at Ka/Q-band with the NASA/POLIMI Alphasat Receiver in Milan, Italy

Michael Zemba¹, James Nessel¹, Lorenzo Luini², Carlo Riva²

¹ NASA Glenn Research Center: Advanced High Frequency Branch, Cleveland, OH, USA

² Politecnico di Milano: Dipartimento di Elettronica, Informazione e Bioingegneria, Milan, Italy

Abstract— Since June of 2014, NASA Glenn Research Center (GRC) and the Politecnico di Milano (POLIMI) have jointly conducted a propagation campaign within the framework of the Alphasat propagation experiment through a propagation terminal at the POLIMI campus in Milan, Italy. The terminal utilizes the 20 GHz and 40 GHz beacons broadcast by the Aldo Paraboni Technology Demonstration Payload (TDP #5), and consists of dual coherent Ka- and Q-band beacon receivers. These provide a direct measurement of the signal attenuation and scintillation and are complemented by concurrent weather instrumentation that provides measurements of the atmospheric conditions at the receiver. The primary goal of these measurements is to improve model predictions of communication system performance at 40 GHz. Over three years of concurrent measurements have now been collected from the terminal, and herein we present a statistical analysis of the results thus far, as well as a summary of recent hardware upgrades to the receivers that were made in September 2017.

Index Terms— *Alphasat, Aldo Paraboni TDP #5, Ka-band, Q-band, radiowave propagation, propagation losses.*

I. INTRODUCTION

While NASA's primary roadmap for future space communications architectures looks toward Ka and optical frequencies, the agency is also investigating available spectrum allocations within the Ka/Q (37 – 42 GHz) and V/W (74 – 84 GHz) bands to meet next generation downlink requirements, specifically as concerning successors to the Tracking and Data Relay Satellite System (TDRSS). As such, NASA Glenn Research Center (GRC) and the Politecnico di Milano (POLIMI) have jointly conducted a propagation campaign measuring rain attenuation, scintillation, and other atmospheric propagation phenomena in Milan, Italy utilizing beacon receivers observing the 20 and 40 GHz beacons onboard the Alphasat TDP#5 Aldo Paraboni Payload. The receivers were installed at the POLIMI campus in Milan, Italy in 2014 atop the Dipartimento di Elettronica, Informazione e Bioingegneria (DEIB) building (Fig. 1, bottom). Instrumentation includes the Ka-band and Q-band beacon receivers (Fig. 1, top), a weather station providing measurements of temperature, pressure, humidity, wind speed and wind direction, a tipping bucket, and a laser disdrometer which yields droplet size and velocity distributions.

Since installation of the Milan station in 2014, two subsequent NASA Alphasat stations have also been deployed:



Fig. 1. Photographs of the Ka/Q-band beacon receivers (above) and overhead view (below) of the receiver location at the POLIMI campus in Milan, Italy.

the first in Edinburgh, Scotland in 2016, and the second in Madrid, Spain in 2017 at the NASA Madrid Deep Space Communications Complex (both of these receive only the 40 GHz Q-band channel). While the fundamental system design remains the same, each subsequent receiver has benefitted from incremental improvements in both hardware and software. The most notable of these is the addition of a digital radiometer measurement, which is accomplished by integrating the noise power captured in the bandwidth surrounding the CW beacon.

To bring the Milan terminal up to date with the receiver design utilized in the more recently deployed terminals, several upgrades were made in September 2017. This paper will

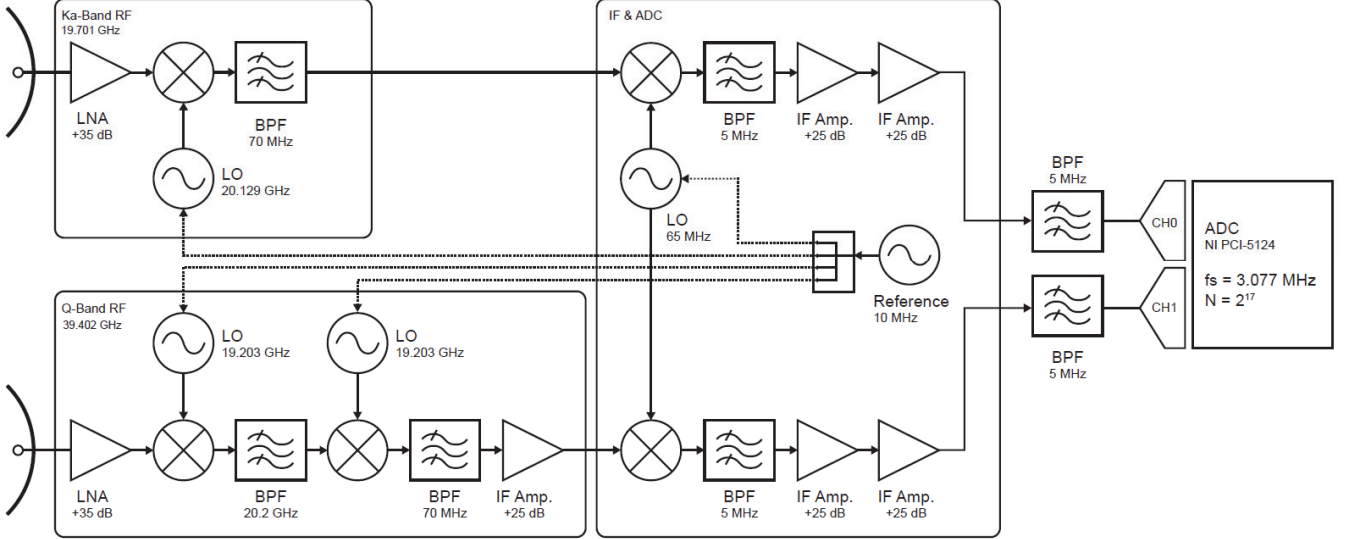


Fig. 2. Block diagram of the revised beacon receiver design, which was updated in 2017 to a final IF of 5 MHz.

introduce the recent hardware and software modifications made to the NASA/POLIMI receiver, as well as investigate the data collected from the system over the first three years of operation.

II. EXPERIMENT DESIGN

A. Ka-/Q-band Beacon Receiver Design

The coherent Ka and Q-band beacon receivers, developed at NASA GRC, utilize a 1.2m Ka-band and a 0.6m Q-band Cassegrain reflector, both with beamwidths of 0.9°. The narrow beamwidth and inclined orbit of Alphasat necessitate active mechanical tracking of the beacons which is accomplished using electronic positioners that update the antenna pointing once per minute within an accuracy of 0.01° in both azimuth and elevation utilizing the Orbital Ephemeris Message (OEM) files for Alphasat. Both the Ka and Q-band channels are downconverted to 70 MHz directly at each antenna's respective feed inside thermally controlled enclosures. Using thermoelectric cooling (TEC) systems, the LNAs, oscillators, mixers, and filters are controlled to within $\pm 0.1^\circ\text{C}$, while the air temperature inside the enclosure remains within $\pm 2^\circ\text{C}$. Both signals are then fed into a common IF enclosure (controlled to within $\pm 1.0^\circ\text{C}$) and further downconverted to 5 MHz, as depicted in the block diagram of Fig. 2. All downconversion stages are referenced to a common ultra-stable 10 MHz citrine oscillator. The IF signal is then digitized and processed utilizing a novel frequency estimation routine to record the frequency and power level of the signals [3], as well calculate the radiometric measurement by integrating the noise power over the available bandwidth of the final downconversion stage (1 MHz). Data is recorded at a measurement rate of 8 Hz, as well as averaged once per minute into 1 Hz measurements. Ultimately, the receivers are able to achieve a dynamic range of approximately 40 dB. The design and characterization of the receivers is further detailed in [4].

B. Recent Receiver Modifications

The current receiver design, incorporating the modifications of 2017, is shown in Fig. 2. The recent modifications were all made within the IF stage: after downconvert to 70 MHz, rather than downconvert to 455 kHz as was originally the case, the final downconverted frequency is now 5 MHz. This change bypasses the previously employed IF downconverter card reused from the propagation terminals of NASA's Advanced Communications Technology Satellite (ACTS), which, although functional, was aging and did not have a wide enough bandwidth to employ the digital radiometer as demonstrated in other receivers. An associated 5 MHz bandpass filter (with a bandwidth of 1 MHz) was added, and two IF amplifiers of 25 dB apiece were added to each channel. The signals are then digitized by the ADC as before, with one more filtering stage at the input to the digitizer.

In software, the sampling frequency and number of points sampled were adjusted to $fs=3.077$ MHz and $N=2^{17}$ to accommodate the higher 5 MHz final frequency. The algorithm for measurement of the signal power, detailed in the next section, remains the same as before, but prior to its application, a notch filter is applied to the beacon and the residual noise power is integrated to compute the digital radiometer measurement. A 1 MHz bandwidth is very narrow as compared to a traditional radiometer measurement, but previous systems such as Edinburgh have demonstrated that radiometric measurements are possible within this design constraint.

III. PROCESSING & DATA ANALYSIS

A. Digital Beacon Receiver

The beacon receiver measurements are accomplished by means of a modified version of the Quinn-Fernandes frequency

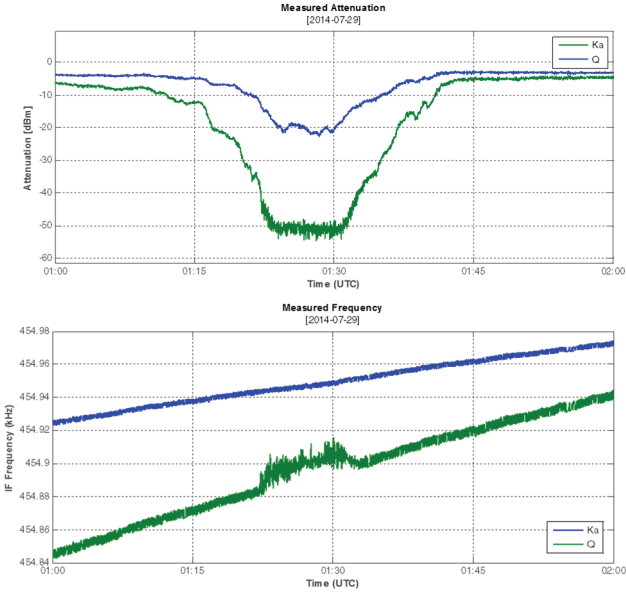


Fig. 3. A rain fade in which the Q channel reaches the receiver noise floor, demonstrating the tracking algorithms and frequency windowing.

estimator. Under normal operation, the Ka and Q channels are independently tracked. When the Q channel fades below a pre-set threshold, the frequency estimator is constrained to a narrow bandwidth centered on the expected Q beacon frequency as derived from the observed Ka-frequency. In practice, this allows for a slightly increased dynamic range at the beginning and end of deep rain fades where the Q beacon is close to or below the receiver noise floor. In Fig. 3, a rain fade is presented where the Q channel experiences a fade beyond the full dynamic range of the receiver, but the Ka channel remains tracked throughout the event. In looking at the frequency (below), it can be seen that the Q channel is limited to a 30 Hz window around the expected frequency. Once the fade passes and the signal level again exceeds the threshold, the frequency estimator returns to a much wider window which allows it to track throughout the longer-term Doppler shift of the frequency. Currently, the zero-reference level calibration is derived from radiosonde measurements collected at Milano Linate Airport and from meteorological information provided by the European Centre for Medium-Range Weather Forecasts (ECMWF).

The digital radiometer measurement added in 2017 is accomplished by notch filtering the beacon using a moving average of past frequency estimates. Both channels are filtered, and the remaining noise power is integrated on both the Ka and Q band channels, independently.

IV. RESULTS

The annual attenuation statistics from June 2014 through December 2017 are shown in Figs. 4 (Ka-band) and 5 (Q-band) in the form of cumulative distribution functions (CDF). Each curve represents the noted calendar year, with the exception of 2014, which is a partial year starting at the commencement of data collection in June. The total attenuation CDF over the entire dataset is also shown. For 99% availability, the associated link margin was 2.98 dB (Ka-band) and 6.39 dB (Q-band).

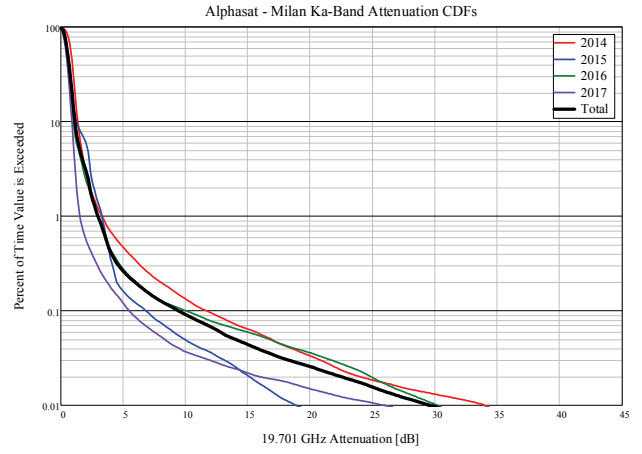


Fig. 4. Cumulative distribution function of observed attenuation by year on the Ka-band channel.

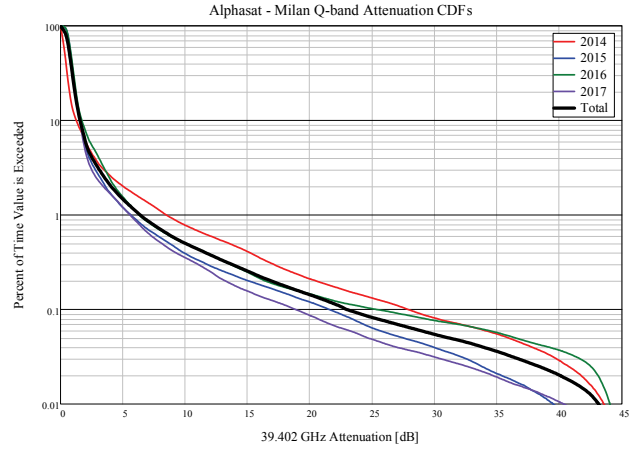


Fig. 5. Cumulative distribution function of observed attenuation by year on the Q-band channel.

TABLE I. OBSERVED ATTENUATION (dB) BY AVAILABILITY

	Ka-Band			Q-Band		
	95%	99%	99.9%	95%	99%	99.9%
Total	1.53	2.98	9.44	2.19	6.39	22.99
2014	1.69	3.31	11.69	2.30	8.50	27.93
2015	2.17	3.31	6.83	2.06	5.65	21.60
2016	1.42	3.01	10.05	2.70	6.31	25.40
2017	1.05	1.54	5.49	1.95	5.58	18.88
January	1.26	1.69	2.72	1.36	2.76	6.76
February	3.03	3.82	4.45	3.59	6.14	12.64
March	0.89	1.95	3.44	2.12	3.77	8.29
April	0.96	1.64	3.45	1.85	5.71	12.52
May	1.05	2.33	5.51	3.07	6.55	19.19
June	1.82	4.36	20.61	2.25	11.25	41.50
July	1.22	2.52	12.34	1.77	6.08	26.78
August	1.29	2.65	13.66	1.80	7.79	30.67
September	1.15	1.89	7.53	1.79	7.32	26.13
October	1.34	2.31	4.80	2.54	6.44	18.75
November	1.81	3.26	7.09	3.43	9.54	20.90
December	0.93	1.22	1.94	1.09	1.95	3.61

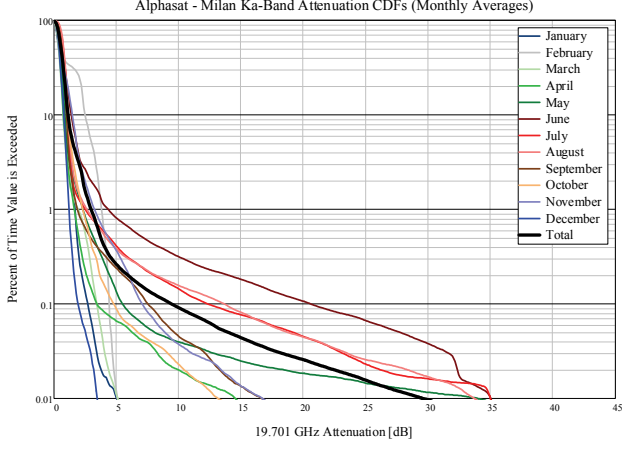


Fig. 6. Cumulative distribution function of observed attenuation by month (from May 2014 through December 2017) on the Ka-band channel.

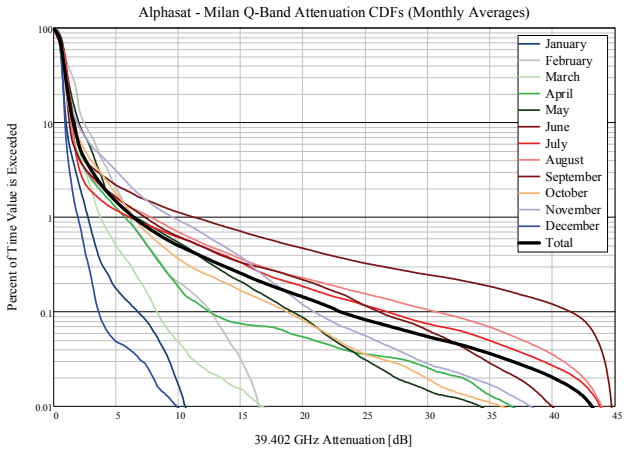


Fig. 7. Cumulative distribution function of observed attenuation by month (from May 2014 through December 2017) on the Q-band channel.

On a monthly basis, the highest attenuation was observed in the wetter summer and fall months (July, August, September) and the smallest attenuation in the drier winter months (December, January, February). Figs. 6 and 7 present the combined monthly CDF curves at Ka and Q band for each calendar month over the currently available period of data collection (June 2014 through December 2017). In December, on average, the margin for 99% availability was 1.22 dB at Ka-band and 1.95 dB at Q-band, while in June, the margin was 4.36 dB at Ka-band and 11.25 dB at Q-band. The observed attenuation for availabilities of 95%, 99%, and 99.9% are highlighted in Table 1, including the total, yearly, and monthly analyses.

An example power spectral density computation demonstrating the performance of the receiver during strong rain fade and scintillation events is shown in Fig. 8 and 9, and as demonstrated, the observed spectral density slope matches well with the theoretically predicted slopes of rain fade and scintillation power spectral density.

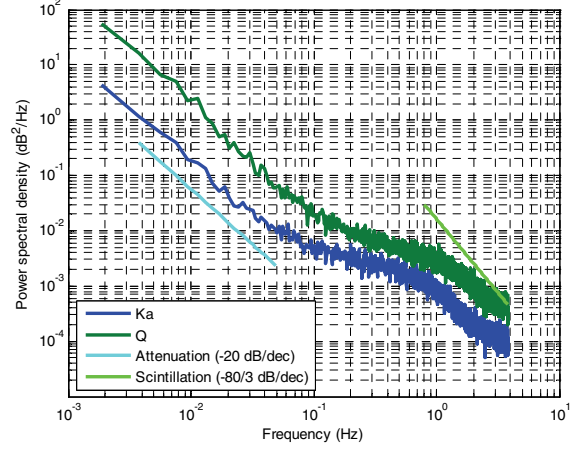


Fig. 8. Power Spectral Density (PSD) of the Ka and Q channel during a heavy attenuation event.

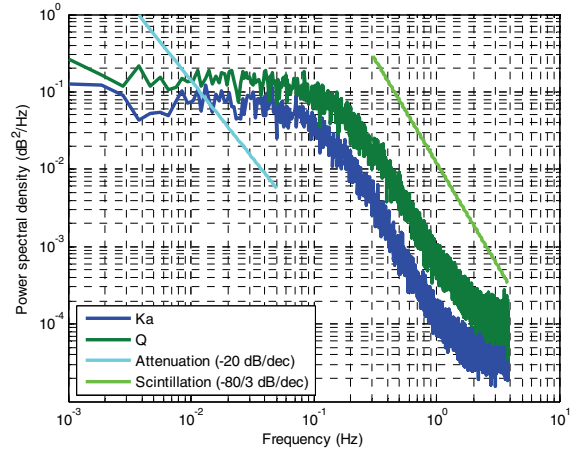


Fig. 9. Power Spectral Density (PSD) of the Ka and Q channel during a strong scintillation event.

V. CONCLUSIONS

Herein we have presented the design, recent improvement, and three-year results from the NASA GRC / POLIMI Alphasat beacon receiver Ka and Q band terminals, which have been collecting data in Milan since 2014. The performance of the receiver has exceeded expectations and has been recording reliable data, and has been recently upgraded to include digital radiometric measurements. We employ a modified Quinn-Fernandes frequency estimation routine to derive the frequency and power measurement of the beacon signals, resulting in a demonstrated dynamic range of approximately 38 dB at the 8 Hz sampling rate, and 45 dB at the 1 Hz sampling rate.

REFERENCES

- [1] D. de Wolf, "On the Laws-Parsons distribution of raindrop sizes," *Radio Science*, Vol. 36, No. 4, pp.639-642, July 2001.
- [2] J. Nessel, M. Zemba, L. Luini, C. Riva, "Comparison of Instantaneous Frequency Scaling from Rain Attenuation and Optical Disdrometer Measurements at K/Q bands", 21st

- Ka and Broadband Communications Conference, Bologna, Italy, October 2015.
- [3] M. Zemba, J. Morse, J. Nessel, "Frequency Estimator Performance for a Software-based Beacon Receiver," IEEE Antennas and Propagation Symposium, July 2014, pp.1574-1575.
 - [4] J. Nessel, J. Morse, M. Zemba, C. Riva, L. Luini, "Preliminary Results of the NASA Beacon Receiver for the Alphasat Aldo Paraboni TDP5 Propagation Experiment," 20th Ka and Broadband Communications Conference, Salerno, Italy, October 2014.
 - [5] Thies Clima Laser Precipitation Monitor: Instructions for Use. Rev. 2.5. July 2011.
 - [6] M. Sadiku, Numerical Techniques in Electromagnetics, 2nd Ed., CRC Press, 2001.
 - [7] C. Bohren, D. Huffman, Absorption and Scattering of Light by Small Particles, Wiley, 1983.
 - [8] H.Y. Lam, J. Din, L. Luini, A. Panagopoulos, C. Capsoni, "Analysis of Raindrop Size Distribution Characteristics in Malaysia for Rain Attenuation Prediction," 2011 URSI General Assembly and Scientific Symposium, August 2011.
 - [9] R. Gunn, G.D. Kinzer, "The terminal velocity of fall for water droplets in stagnant air," Journal of Meteorology, Vol. 8, pp.249-253, 1949.
 - [10] S. Bertorelli and A. Paraboni, "Modelling of short-term frequency scaling for rain attenuation using ITALSAT data," Int. J. Satell. Commun., vol. 25, no. 3, pp. 251–262, 2007.
 - [11] G. Karagiannis, A. D. Panagopoulos, J. D. Kanellopoulos, "Short-Term Rain Attenuation Frequency Scaling for Satellite Up-Link Power Control Applications", IEEE Transactions on Antennas and Propagation, vol.61, Issue 5, May 2013.
 - [12] D.E. Setzer, "Computer transmission through rain at microwave and visible frequencies," Bell Syst. Tech. J, vol. 49, no. 8, Oct. 1970, pp.1873-1892.